Chinese Journal of Chemical Engineering 53 (2023) 260–269

Contents lists available at ScienceDirect

Chinese Journal of Chemical Engineering

journal homepage: www.elsevier.com/locate/CJChE

Full Length Article

Dissolution behavior, thermodynamic and kinetic analysis of malonamide by experimental measurement and molecular simulation

Peng Yang [1,#], Shengzhe Jia [1,#], Yan Wang [2], Zongqiu Li [1], Songgu Wu [1,*], Jingkang Wang [1], Junbo Gong [1]

[1] School of Chemical Engineering and Technology, State Key Laboratory of Chemical Engineering, Tianjin University, Tianjin 300072, China
[2] School of Pharmaceutical Sciences (Shandong Analysis and Testing Center), Qilu University of Technology (Shandong Academy of Sciences), Jinan 250014, China

ARTICLE INFO

Article history:
Received 11 October 2021
Received in revised form 6 March 2022
Accepted 10 March 2022
Available online 4 April 2022

Keywords:
Malonamide
Solubility
Thermodynamic properties
Molecular simulation
Nucleation rate

ABSTRACT

In this study, the solid structure, dissolution behavior, thermodynamic properties and nucleation kinetics of malonamide were explored. Firstly, the Hirshfeld surface analysis and molecular electrostatic potential surface were plotted to reveal the percentage contribution of various intermolecular contacts and location of the strongest hydrogen bond. Next, the solubility of malonamide in 12 solvents was determined by dynamic method at temperatures from 278.15 K to 318.15 K. Four thermodynamic models were applied to analyze solubility results. In addition, the thermodynamic properties were calculated to further analyze and discuss the dissolution behavior of malonamide. Moreover, the physicochemical properties of solvents were explored to express the solvent effects. The results illustrate "like dissolves like", "mass transfer" and "solvent–solute interaction" rules play the synergistic effects on the dissolution process. The molecular dynamic simulation, including radial distribution function analysis and solvent free energy, was used to further explain the dissolution behavior. At last, the nucleation rate and effective interfacial energy in methanol solvent was measured and calculated to reveal the nucleation behaviour.

1. Introduction

Malonamide (as shown in Fig. 1, $C_3H_6N_2O_2$, CAS registry NO. 108-13-4), is often used as an intermediate compound to produce the pharmacologically active derivatives in the pharmaceutical field [1,2]. Several derivatives of malonamide have been patented for some disease treatment, such as treatment for sebaceous gland disorders and cardiovascular disorders. So far, three crystal forms: form I (monoclinic system), form II (tetragonal system), form III (orthorhombic system), have been reported, and the calculated morphology is shown in Fig. S1 in Supplementary Material. Among three crystal forms, the other two crystal forms can be prepared by stable form I [3]. To be specific, the form III can be prepared by melting the form I at 184 °C, and allowing the sample to cool down to room temperature in the oven. The form II can be obtained by two approaches: solid state grinding or annealing above 136 °C, and both the two approaches are used form I as the raw materials.

In pharmaceutical field, solution crystallization is proved as an efficient pathway to improve the crystal products performance and optimize the physical properties of the crystal products, such as purity and crystal morphology, *etc.* Moreover, the crystal features not only deeply affect the downstream handling and processing, but end-use functional properties, such as filterability, flowability *etc.* [4–6]. For example, the flack-shape and long needle-shape crystals are not desirable. The former tends to form an impermeable layer, which is not benefit for filtration and washing. The latter morphology seriously impacts the blending process and the final tableting operation because of the poor flowability. While, block-like crystals are welcome in the industrial production, especially in the pharmaceutical field, which filter and blend more readily. As a result, developing efficient approaches to prepare the desired characteristics of the product has gained wide interests. Crystallization has been demonstrated as an efficient crystal quality improvement method [7–9]. Solubility is an essential parameter during the solution crystallization, determining the equilibrium state and optimized operational trajectory. It is also significant for the crystallization conditions selection, process optimization, and designing solution crystallization pathways.

In this study, the malonamide (form I) is chosen as the model compound. The solid-state properties are firstly investigated to analyze the intermolecular interaction in malonamide crystals. Then, the solubility of malonamide in 12 common solvents is researched by dynamic methods from 278.15 K to 318.15 K. Four thermodynamics models are introduced to fit and analyze the

* Corresponding author.
E-mail address: wusonggu@tju.edu.cn (S. Wu).
# These authors contributed equally to this work.

https://doi.org/10.1016/j.cjche.2022.03.012
1004-9541/

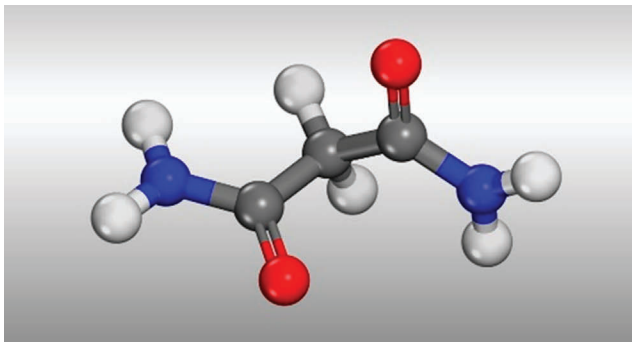

Fig. 1. Molecular structure of malonamide.

experimental outcomes, and the mixing properties are also calculated to analyze the dissolution behavior of malonamide. Furthermore, the molecular simulation, including solvent free energy and radial distribution function, are applied to further analyze solubility results. At last, the nucleation dynamic parameters of malonamide: nucleation rate and effective interfacial energy, are also investigated in methanol system.

2. Experimental

2.1. Materials

Malonamide (mass fraction $\geq$ 99.0%) was supplied by Shanghai Aladdin Biochemical Technology Co., Ltd. (China). The solvents were supplied by Tianjin Kemiou Chemical Technique Co., Ltd. (China) with purity >99.5%. The detailed information of solute and solvents are presented in Table S1 (See Supplementary Material).

2.2. Powder X-ray diffraction and thermal analysis

The powder X-ray diffraction (PXRD) was applied to analyze the solid form of malonamide during the experiments. The PXRD patterns were collected by D/MAX-2500 (Rigaku, Japan) with Cu K_α radiation (0.15405 nm) over the diffraction angle (2θ) rang of 2°–40° at the speed of 8° min^{-1}. The differential scanning calorimeter (DSC 1, Mettler-Toledo, Switzerland) was applied to characterize thermodynamic properties of the malonamide. About 5 mg malonamide was heated from 303.15 K to 473.15 K at a heating rate of 10 K·min^{-1}.

2.3. Solubility measurements

In this study, the solubility of malonamide in 12 solvents was investigated by the dynamic approach from 278.15 K to 318.15 K [10,11]. The dissolution process was detected by a laser monitoring system containing laser generator, the photoelectric transformer and the light intensity display and the temperature was regulated by a thermostatic water bath (CF41, Julabo, Germany). During the dissolution process, the temperature was monitored by the electronic thermometer, and the standard uncertainty is 0.1 K. The mass of the solvent and solute was measured by an analytical balance (ML204, Mettler-Toledo, Switzerland), and the standard uncertainty is 0.0001 g. Firstly, at least 20 g solvent was added to the test tube. Then, the test tube was placed on the magnetic agitator with the stirring speed of 400 r·min^{-1}. At the same time, the laser system proceeded to monitor the dissolution process, in which the laser beam index intensity changed with the dissolution process simultaneously. The intensity increased with particles dissolution, and the intensity reached its maximum when the particles dissolved totally. At first, the intensity dropped sharply when the solute was added, and rose tenderly during the process of dissolution, and reached the peak after the solute was completely dissolved. Next, additional solute (less than 2 mg) was supplied into the test tube and the laser intensity dramatically decreased, then increased slowly as the dissolution of solute. This procedure was repeated for some times until the intensity beam dropped and maintained at a constant value for at least 5 h after the last addition. When the strength value did not reach a relatively constant maximum, the system was considered to achieve the solid–liquid equilibrium state. The mass of the malonamide put into the tube was recorded as m_1, and the mass of solvent was recorded as m_2, the solubility x_1 can be obtained by Eq. (1), where M_1 and M_2 were the molecular weight of solute and solvent, respectively.

$$x_1 = \frac{m_1/M_1}{m_1/M_1 + m_2/M_2} \tag{1}$$

2.4. Intermolecular interactions analysis

2.4.1. Hirshfeld surface analysis

As the convenient and efficient tool, Hirshfeld surface and 2D fingerprint were introduced to determine the intermolecular interactions of malonamide. The Crystal Explorer 17.5 software was adopted to obtain the plots of malonamide at B3LYP/6-31G(d) level [12].

2.4.2. Molecular electrostatic potential surface (MEPS)

MEPS was extensively used to describe the overall distribution of intermolecular charges and intermolecular interactions. The molecular structure of malonamide was optimized and performed by Density Functional Theory with the B3LYP hybrid functional at 6-311G (d, p) and 6-311+G (d, p) level in Gaussian 09 software, and the results were analyzed by Multiwfn software [13].

2.5. Molecular simulation

2.5.1. Solvation free energy

As an effective parameter, solvation free energy, is used to analyze the interaction between the solute and solvent, which refers to the energy change of solute phase when transfers from vapor to the solvent phase. The Dmol3 module in Material Studio was applied to obtain the construct files. The solute and solvent molecular structures were optimized, and the energy file was obtained. Then, the molecular structure was optimized by COSMO Solvation model and the solvation free energy was calculated by COSMOtherm software [14,15].

2.5.2. Radial distribution function (RDF) analysis

RDF represents the appearing frequency of atoms for a specific atom at a distance, which can be used to investigate the interaction between molecules. The RDF analysis was conducted by Material Studio software with the force field of COMPASS (Condensed-phase Optimized Molecular Potentials for Atomistic Simulation Studies) along with the forcefield assigned charges. The electrostatic interaction was calculated by the Ewald method with an accuracy of 0.418 J·mol^{-1}, and the van der Waals interaction was calculated by the atom-based method with a cutoff distance of 1.55 nm. The supercell with dimensions of larger than 3.1 nm was built in Amorphous Cell module by malonamide and solvent molecules based on the solubility of malonamide at 298.15 K. After the geometry optimization of supercell, the dynamic simulation was proceeded with NVT and NPT ensemble (constant particle numbers (N), volume (V), pressure (P) and temperature (T)) in turn

for 1000 ps at 298.15 K and 101.3 kPa in Forcite module. At last, RDF results could be obtained from the simulation trajectory [16,17].

2.6. Nucleation kinetics

Moreover, the nucleation kinetics of malonamide was also researched under different supersaturations. The solubility data in methanol were employed to prepare solution with different supersaturations [18–20]. The supersaturation S is defined as x^*/x, where x^* is the real mole fraction, and x is the equilibrium solubility value under the temperature points. In this study, four supersaturations: 1.15, 1.2, 1.3 and 1.4 were chosen to investigate the nucleation rate and kinetics parameters. At the beginning, appropriate amounts of malonamide and 40 ml methanol were transferred into a 50 ml beaker to form the stock solution. The stock solution was kept at 318.15 K by a thermostatic bath, and stirred at 200 r·min^{-1} for few hours. After the malonamide was dissolved, 3 ml solution was filtered by the syringe filter (0.22 μm) and dispensed into a 10 ml glass vial with the plastic capsule to avoid solvent evaporation. The glass vial was maintained at 318.15 K for 2 h with the stirring speed of 200 r·min^{-1} to avoid the thermal history effect. Then, the glass vial was moved to a jacketed crystallizer controlled at 293.15 K to create the supersaturation for nucleation, and the agitation was kept at 200 r·min^{-1}. The induction time was considered as the interval between the time when the supersaturation was established and the time when the nuclei appear. The nuclei appearance was observed by a digital USB optical microscope. For each supersaturation, the induction time was measured for 80 times to obtain the probability distribution.

3. Thermodynamic Models

To better examine the solubility results, four thermodynamics models are introduced to analyze the solubility data. Meanwhile, the thermodynamic properties are also obtained by the NRTL (non-random two liquids) model.

3.1. Apelblat equation

Apelblat equation is considered as a semiempirical model and used to evaluate the correlation between temperature and mole solubility [21], as listed in Eq. (2).

$$\ln x_1 = A + B/T + C\ln T \tag{2}$$

where T refers to the absolute temperature, and A, B and C are the process parameters, which are closely related with the solution and enthalpy effects.

3.2. λh equation

The λh Eq. (3) is adopted to explain the solubility rules in the solvent of choice according to the solid–liquid equilibrium [22,23].

$$\ln\left(1+\frac{\lambda(1-x_1)}{x_1}\right) = \lambda h\left(\frac{1}{T}-\frac{1}{T_m}\right) \tag{3}$$

T_m and T are the melting point of malonamide and absolute temperature of the system, respectively. λ and h are the parameters of the equation.

3.3. NRTL model

NRTL model is introduced to describe and explain the excess Gibbs energies of nonideal mixtures [24,25]. The model can be presented by Eqs. (4)–(7).

$$\ln\gamma_i = x_j^2\left[\frac{\tau_{ji}G_{ji}^2}{(x_i+G_{ji}x_j)^2}+\frac{\tau_{ij}G_{ij}}{(x_j+G_{ij}x_i)^2}\right] \tag{4}$$

$$G_{ij} = \exp(-\alpha_{ij}\tau_{ij}) \tag{5}$$

$$\alpha_{ij} = \alpha_{ji} = \alpha \tag{6}$$

$$\tau_{ij} = (g_{ij}-g_{jj})/RT \tag{7}$$

γ_i is the activity coefficient. τ_{ij} and τ_{ji} are the equation dimensionless interaction parameters. g_{ij} and g_{jj} stand for the interaction energy parameters. α_{ij}, α_{ji} and α are relate with non-randomness in the mixture, which can be adjusted between 0.2 and 0.47.

3.4. van't Hoff equation

At last, van't Hoff equation Eq. (8) is introduced to calculated the correlations between mole fraction solubility and the absolutely temperature [26].

$$\ln x_1 = a/T + b \tag{8}$$

where a and b represent the fitting parameters related to the enthalpy and entropy of the solution.

4. Results and Discussion

4.1. Characterization of malonamide

To determine the crystal form of malonamide during the dissolution process, excess amount of the malonamide was added in the twelve solvents for at least 6 h under 400 r·min^{-1}. Then, the suspension particles were characterized by the PXRD. The patterns of PXRD shown in Fig. 2 indicate that the malonamide remains the same solid form during the experiments.

The melting enthalpy and melting point of the malonamide was measured by the differential scanning calorimeter (DSC), and the result is presented in Fig. 3. The melting point (T_m) and melting enthalpy ($\Delta_{fus}H$) of malonamide obtained by DSC are (440.67 ± 0.5) K and 29.08 kJ·mol^{-1} (with 1.454 kJ·mol^{-1} uncertainty at 0.95 level) respectively, which are consistent with Ref. [2].

4.2. Hirshfeld surface analysis

In this section, the solid properties of malonamide were revealed by the Hirshfeld surface analysis. This analysis method is an essential tool to calculate and interpret the intermolecular interaction without changing the molecule structure. 2D fingerprint plots are applied to emphasize particular close contact, visualize the intermolecular interactions of malonamide crystal where d_e and d_i are the distances of points on surface to the nearest external and internal atoms, respectively [27–30].

The 2D fingerprint patterns and the main percentage of relative intermolecular interactions of the malonamide are shown in Fig. 4. Obviously, the O···H contact is the dominated interaction, accounting for 50.3% to the Hirshfeld surface. Next, the H···H contact also plays the significant role in the crystal structure of malonamide, and comprises 33.5% of the Hirshfeld surface area. It seems that the molecular surface is formed by a sea of H and O atoms. Other weak intermolecular interaction: N···H, C···H and O···N contact, can contribute to 7.0%, 5.1% and 2.5% of the Hirshfeld surface area, respectively.

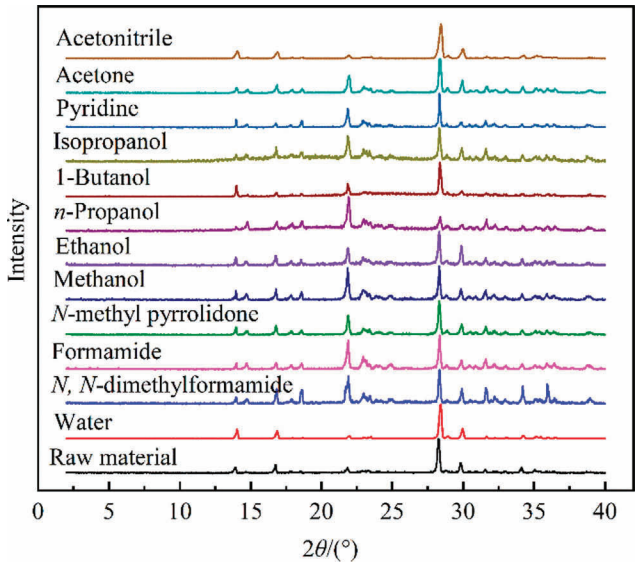

Fig. 2. The PXRD patterns of malonamide.

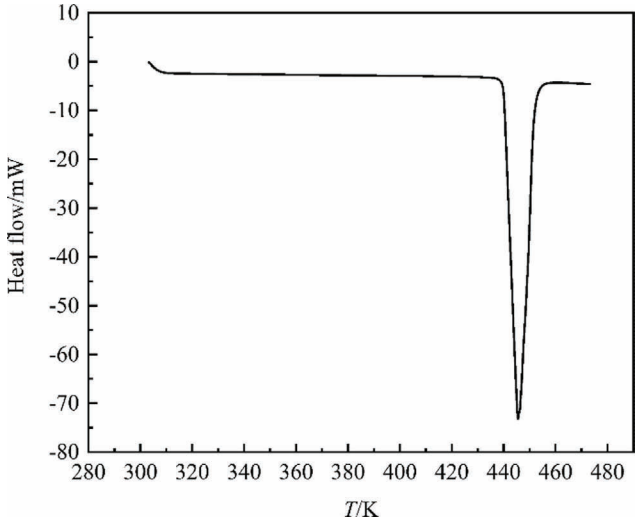

Fig. 3. DSC curve of the malonamide.

4.3. Molecular electrostatic potential analysis (MEPS)

The MEPS of malonamide is presented in Fig. 5, where the blue area stands for the positive potential surface of malonamide and the red area is the negative potential surface [12]. It can be found that the most negative potential of malonamide is shown around the O atom (−152.99 kJ·mol^{-1}), while the most positive potential is observed around N atom (169.88 kJ·mol^{-1}). With hydrogen bond donors and acceptors, the malonamide molecules are more likely to make the hydrogen bonding interaction with several solvents, which can promote the dissolution process of solute.

4.4. Solubility determination

The solubility of the malonamide in twelve solvents is investigated from 278.15 K to 318.15 K by the dynamic method. The solubility results at different measured points are presented in Table S2 and Fig. 6. Apparently, all the solubility data increase with the temperature increases for the reason that the intermolecular interaction between the solute and solvent increases with increasing the temperature. The malonamide shows large solubility in *N*-methyl pyrrolidone and *N*,*N*-dimethylformamide systems, while exhibits very slight dissolution capacity in acetonitrile and acetone systems. Besides, the solubility of malonamide in water, *N*,*N*-dimethylformamide, formamide and *N*-methyl pyrrolidone is much higher than that in other eight solvents. For five alcohol systems, the malonamide possesses the highest solubility in methanol system, which is far higher than other four solvent systems, followed by ethanol system. The solubility data in *n*-propanol, isopropanol and 1-butanol are relatively close.

4.5. Data analysis and thermodynamic properties

Two calculated parameters: average relative deviation (ARD) and root mean square deviation (RMSD), are used to examine the experimental results and the applicability of the models, listed in Eqs. (9), (10), where x_i^{exp} and x_i^{cal} are the experimental and fitting solubility, and N is the number of experimental points.

$$\mathrm{ARD} = \frac{1}{N}\sum_{i=1}^{N}\left|\frac{x_i^{exp} - x_i^{cal}}{x_i^{exp}}\right| \tag{9}$$

$$\Delta_{mix}S^{id} = -R(x_1 \ln x_1 + x_2 \ln x_2) \tag{10}$$

The ARD and RMSD values and the fitting parameters of four thermodynamic models are summarized in Tables S3–S6. The biggest ARD value is less than 7% in four thermodynamics models, indicating an accurate measured result. The Apelblat equation possesses the best fitting outcomes with smallest ARD values.

Moreover, the thermodynamic properties of the malonamide in twelve solvents: mixing enthalpy ($\Delta_{mix}H$), mixing Gibbs free energy ($\Delta_{mix}G$) and mixing entropy ($\Delta_{mix}S$), are obtained by NRTL model [31,32]. The mixing properties could be analyzed based on Eqs (11)–(13).

$$\Delta_{mix}G^{id} = RT(x_1 \ln x_1 + x_2 \ln x_2) \tag{11}$$

$$S^E = \frac{H^E - G^E}{T} H^E = -T^2\left[\frac{\partial(G^E/T)}{\partial T}\right] \tag{12}$$

$$\Delta_{mix}H^{id} = 0 \tag{13}$$

where $x_1$and x_2 mean the mole fraction of the solute and solvent.

In real solvent systems, the mixing properties: $\Delta_{mix}G$, $\Delta_{mix}S$ and $\Delta_{mix}H$, can be calculated by Eqs (14)–(16). G^E, S^E and H^E are the excess properties, which can be obtained by Eqs (17)–(19).

$$\Delta_{mix}G = G^E + \Delta_{mix}G^{id} \tag{14}$$

$$\Delta_{mix}S = S^E + \Delta_{mix}S^{id} \tag{15}$$

$$\Delta_{mix}H = H^E + \Delta_{mix}H^{id} \tag{16}$$

$$G^E = RT(x_1 \ln\gamma_1 + x_2 \ln\gamma_2) \tag{17}$$

$$H^E = -T^2\left[\frac{\partial(G^E/T)}{\partial T}\right] \tag{18}$$

$$S^E = \frac{H^E - G^E}{T} \tag{19}$$

where γ_1 and γ_2 are the activity coefficient for the components in real solution. The outcomes of $\Delta_{mix}G$ are provided in Table S7 and Fig. 7. All the $\Delta_{mix}G$ values are negative, showing that the mixing process is a spontaneous process. Besides, the $\Delta_{mix}G$ values in water, dimethyl formamide, formamide and *N*-methyl pyrrolidone systems are more negative than the other systems, which is corre-

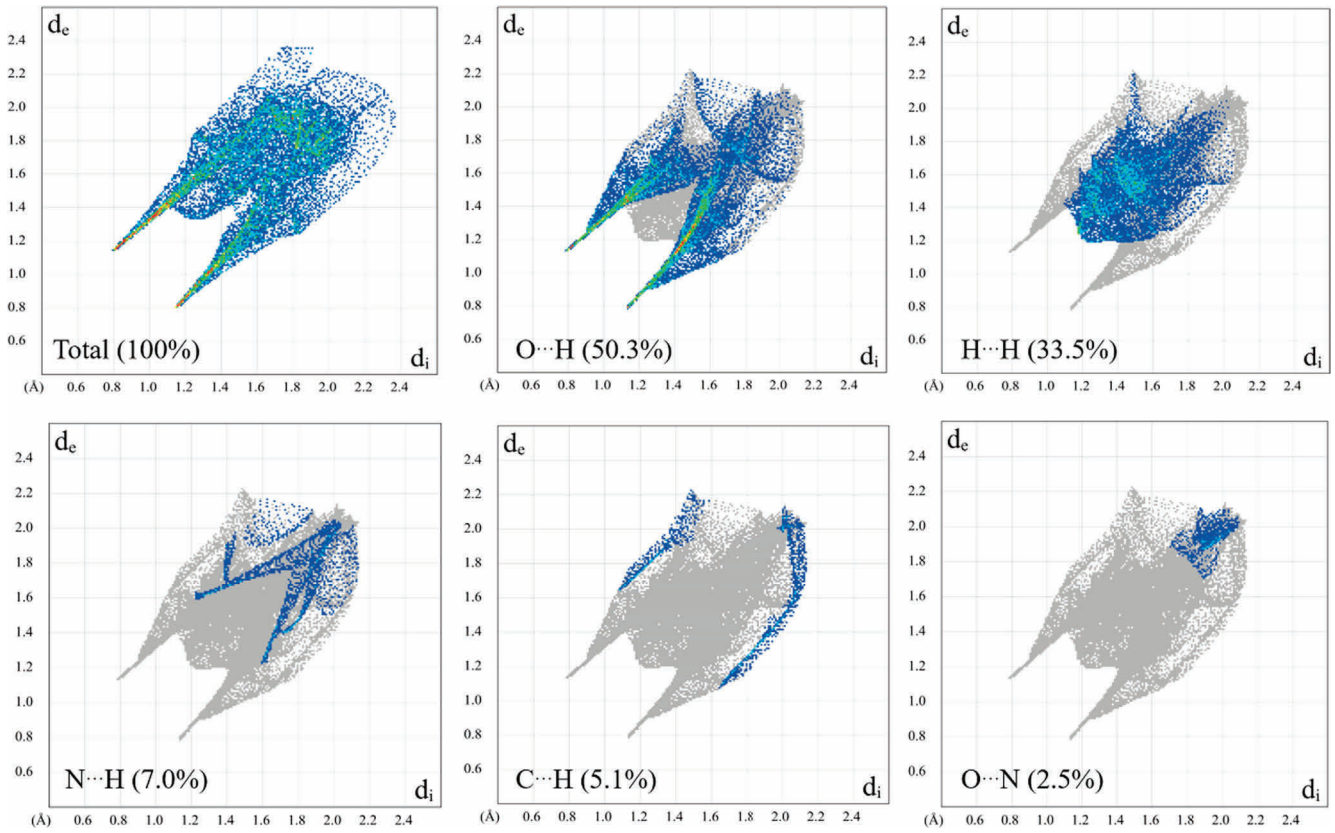

Fig. 4. 2D fingerprint plots of malonamide (1 Å=0.1 nm).

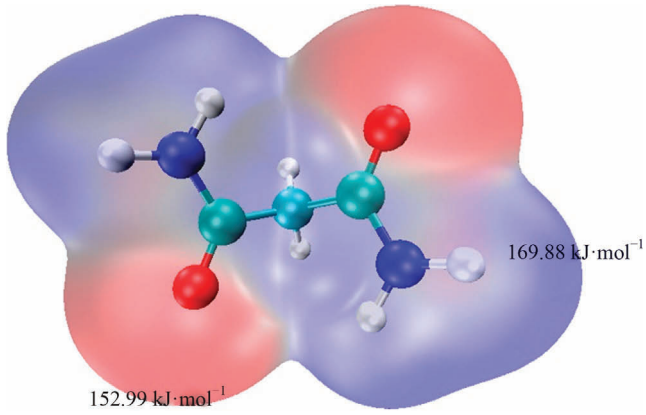

Fig. 5. The MEPS of malonamide.

sponding with higher solubility in the four solvent systems. All the absolute values of $\Delta_{mix}G$ increase with the temperature, illustrated that increasing temperature favors the dissolution process [26].

The $\Delta_{mix}S$ results calculated from the NRTL model are presented in Fig. 8 and listed in Table S7. All the $\Delta_{mix}S$ values increase with the temperature, and the $\Delta_{mix}S$ in water, dimethyl formamide, formamide and *N*-methyl pyrrolidone systems are much higher than the other solvent systems.

4.6. Solvent effects analysis

In this study, the model compound, malonamide possesses hydrogen acceptor and donor groups, which means that it may exhibit higher solubility in the higher polarity solvent systems. Besides, other solvent effects could also be considered to determine the dissolving processes [27,33]. Therefore, several solvent properties: cohesive energy density, polarity, hydrogen bond donor and acceptor ability, dielectric constant and viscosity at 298.15 K are shown in Table S8, to explain the dissolution behavior [34,35]. The solubility results effected by physicochemical properties in five alcohol systems are shown in Fig. 9. Except for the 1-butanol and *iso*-propanol systems, the solubility values in other systems increase with the solvent polarity, as listed in the following sequence: methanol > ethanol > *n*-propanol, which can be interpreted by the "like dissolves like" principle [36]. Besides, the viscosity of the alcohol solvents is also investigated to explain the dissolution rules. Higher viscosity can cause higher mass transfer resistance, resulting in lower solubility values. For the methanol and ethanol systems, the two solvents possess the highest polarity but lowest viscosity among the five alcohol systems. So, the malonamide displays higher solubility in methanol and ethanol. However, the polarity and viscosity rules cannot explain the solubility result in 1-butanol solvent, and the cohesive energy density is proposed to analyze the dissolution process in the butanol system. Higher value means higher solvent–solvent interactions but lower solvent–solute interactions, causing lower solubility values [37,38]. 1-Butanol possesses the lowest cohesive energy density, causing the higher solute–solvent interactions and higher solubility value. Overall, the solubility results are caused by several intermolecular interactions and solvent properties, and single kind of intermolecular interaction may not explain the solubility results accurately.

4.7. Molecular dynamic simulation

RDF analysis and solvation free energy are introduced to better explain the dissolution behavior and visualize the solubility difference.

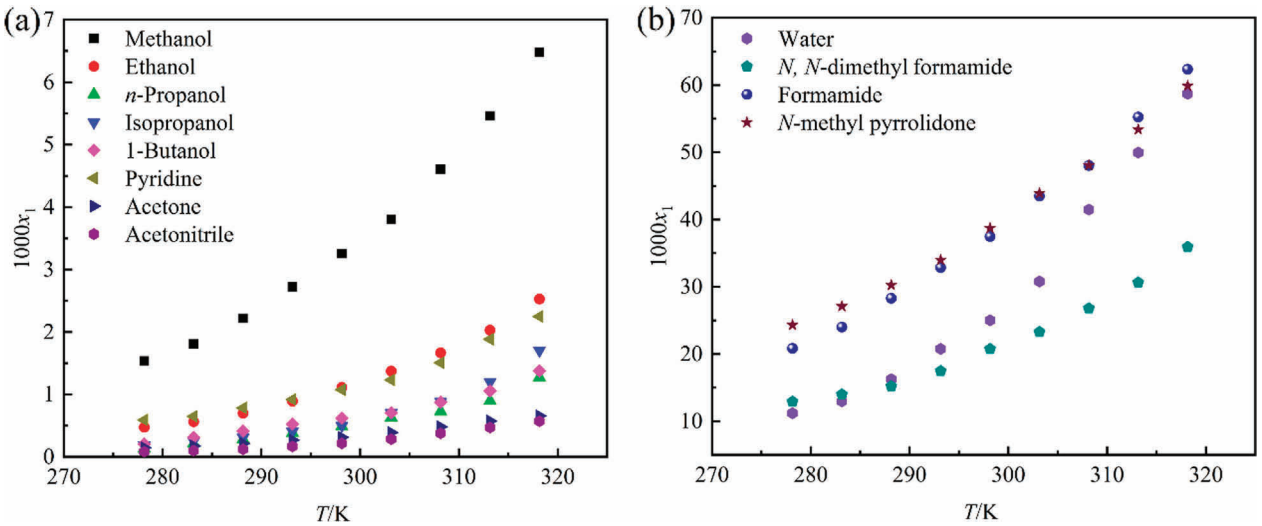

Fig. 6. The solubility values of malonamide at experimental temperatures.

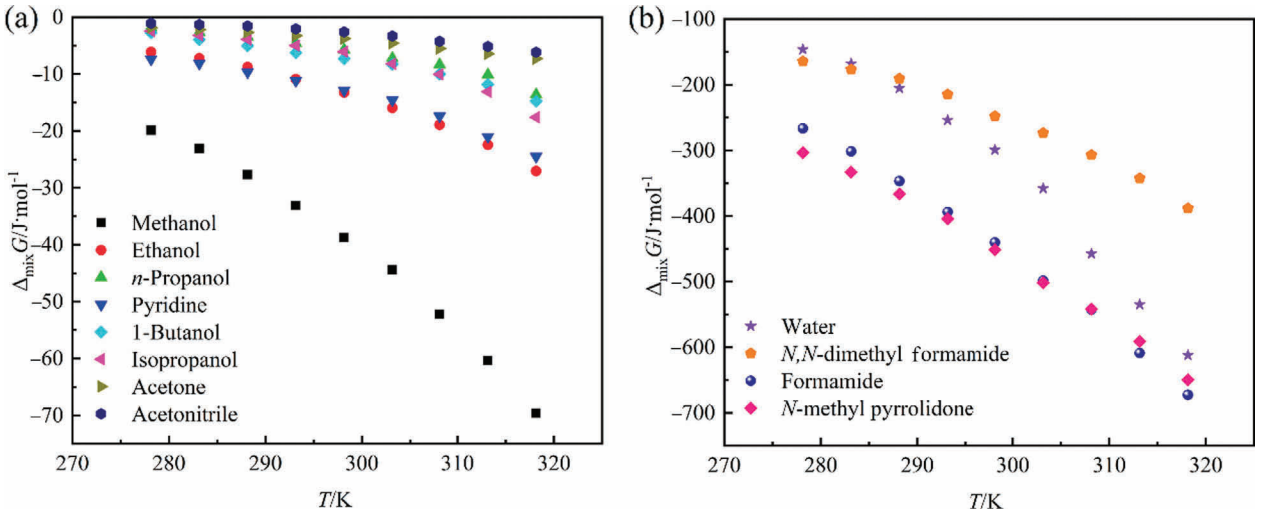

Fig. 7. The $\Delta_{mix}G$ of malonamide in experimental solvents.

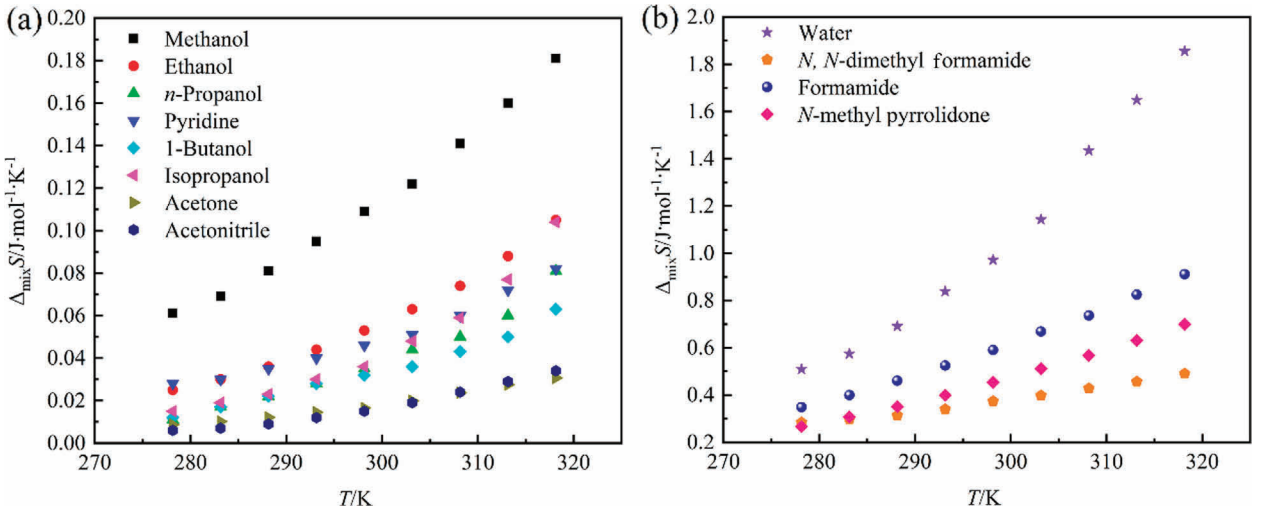

Fig. 8. The mixing entropy of malonamide in experimental solvents.

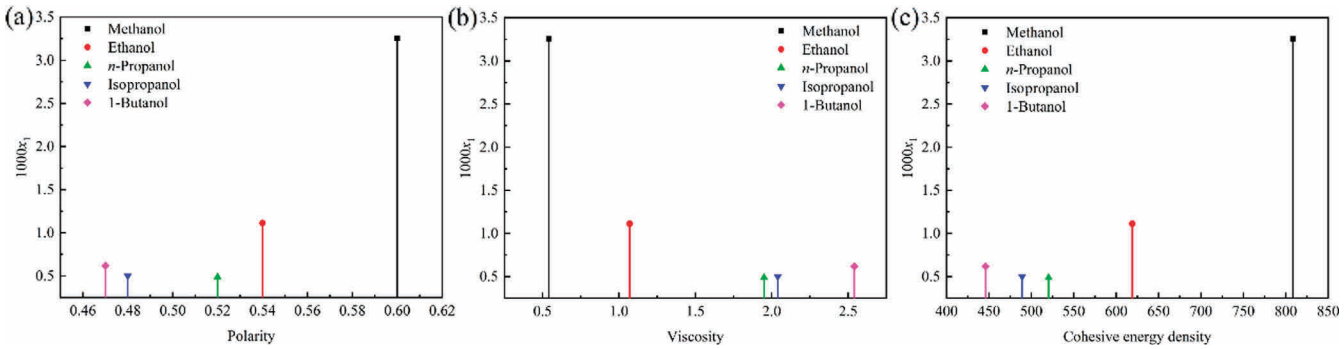

Fig. 9. The solubility of malonamide in alcohols at 298.15 K as a function of (a) polarity, (b) viscosity and (c) cohesive energy density.

4.7.1. RDF analysis

RDF analysis is a resultful method to display the interaction of chosen atoms. In the RDF diagram, a peak located at 0.15–0.3 nm stands for the formation of hydrogen bond between the chosen atoms. Generally, higher hydrogen bond represents stronger hydrogen bonding, causing higher solubility value. In this section, several solvent systems: methanol, ethanol, acetone and acetonitrile are chosen to research the hydrogen bonding values. As shown in Fig. 10, three kinds of hydrogen bond are formed including O—H···O, O···H—N and O—H···N in methanol and ethanol systems, for the reason that the hydroxy group in alcohol acts as both a hydrogen bond donor and acceptor. However, only one kind of hydrogen bond are formed in the acetone and acetonitrile systems (O···H—N for acetone and N···H—N for acetonitrile), for the reason that there is no hydrogen bond donor in acetone and acetonitrile. Besides, the strongest hydrogen bond O—H···O in the methanol and ethanol systems are formed by hydroxyl group in alcohol solvents and O atom in carbonyl of malonamide, which is much stronger than the hydrogen bond formed by malonamide and acetone/acetonitrile solvents. Thus, the solubility data of malonamide in the alcohols are much larger than that in acetone and acetonitrile. Moreover, the solubility values in methanol are also larger than those in the ethanol solvent for the reason that the hydrogen bond between methanol and malonamide shows the higher intensity.

4.7.2. Solvation free energy (SFE)

SFE is applied for representing the strength of the interaction between solute and solvent. Therefore, the large value of the SFE can result in stronger solute–solvent interaction, causing higher solubility value. In this study, six common solvation free energies (water, methanol, methanol, 1-propanol, acetone, acetonitrile) are calculated and listed in Table 1.

The correlation between the absolute value of SFE with solubility value is also presented in Fig. 11. The solubility value increases with the absolute value of SFE due to the increase of the solute–solvent interaction.

To sum up, generally, the solubility increases with the polarity of solvent, and decreases with the viscosity and coherence energy density of solvent. Meanwhile, available molecular dynamic simulation can also explain the solvent effects and solubility results. For example, solubility can show an increase tendency with the solvation free energy. Notably, the solubility is determined by several factors, such as intermolecular interactions and solvent properties, and single variable may not explain the solubility results accurately.

4.8. Nucleation kinetics

At last, the nucleation behavior of the malonamide in methanol was also calculated at four different supersaturations. The nucleation rate was calculated by the probability method. The correlations between the probability distribution and induction time could be calculated by the Eq. (20) [39–41].

$$P(t) = 1 - \exp(-JVt) \tag{20}$$

where $P(t)$ refers to the nucleation probability, J and V are the steady-state nucleation rate and solution volume, and t means the induction time. Eq. (20) can be transferred into Eq. (21).

$$-\ln(1 - P(t))/V = Jt \tag{21}$$

The fitting linear correlations of Eq. (21) are presented in Fig. 12, and the nucleation rate and R^2 of the fitting results are listed in Table 2. All R^2 are more than 0.985, illustrating good fitting results.

Next, the correlation between nucleation rate and supercooling degree is also calculated based on the Eq. (22), where A and B are the kinetics and thermodynamics parameters [42,43]. The parameter B can express the energy barrier for nucleation. Besides, the parameter B can be calculated by Eq. (23), where γ, v and k are effective interfacial energy, molecular volume and Boltzmann constant, and T is 293.15 K.

$$J = A\exp\left(-\frac{B}{\ln^2 S}\right) \tag{22}$$

$$B = \frac{16\pi\gamma^3 v^2}{3(kT)^3} \tag{23}$$

When plotting ln$J$ *versus* $-1/\ln^2 S$, the straight line can also be yielded, and the results are shown in Fig. 13. Furthermore, based on the Eq. (23), the effective interfacial energy is calculated as 2.35 mJ·m^{-2}.

5. Conclusions

This study explored the solid-state structure, thermodynamic and kinetics properties of the malonamide. Firstly, the Hirschfeld surface analysis was introduced to point out the contribution of different intermolecular contacts in crystal structure. The results indicate the malonamide molecule is surrounded by a lot of the O and H atoms, and O···H and H···H interactions are dominant in crystal structure. The molecular electrostatic potential was also applied to analyze and calculate the molecular electrostatic potential surface, indicated that the strongest hydrogen bond is located at the O atom. Secondly, the solubility of malonamide in 12 solvents was investigated by the dynamic method from 278.15 K to 318.15 K. Furthermore, four thermodynamics models were adopted to evaluate the solubility data. All the *ARD* values in the four models are less than 7%, indicating good fitting performance. Several mixing properties were also calculated using the NRTL model. All the $\Delta_{mix}G$ are negative, while all the $\Delta_{mix}S$ are positive, indicating the dissolution behavior is a spontaneous process. Moreover, all the $|\Delta_{mix}G|$ and $|\Delta_{mix}S|$ values increase with the tempera-

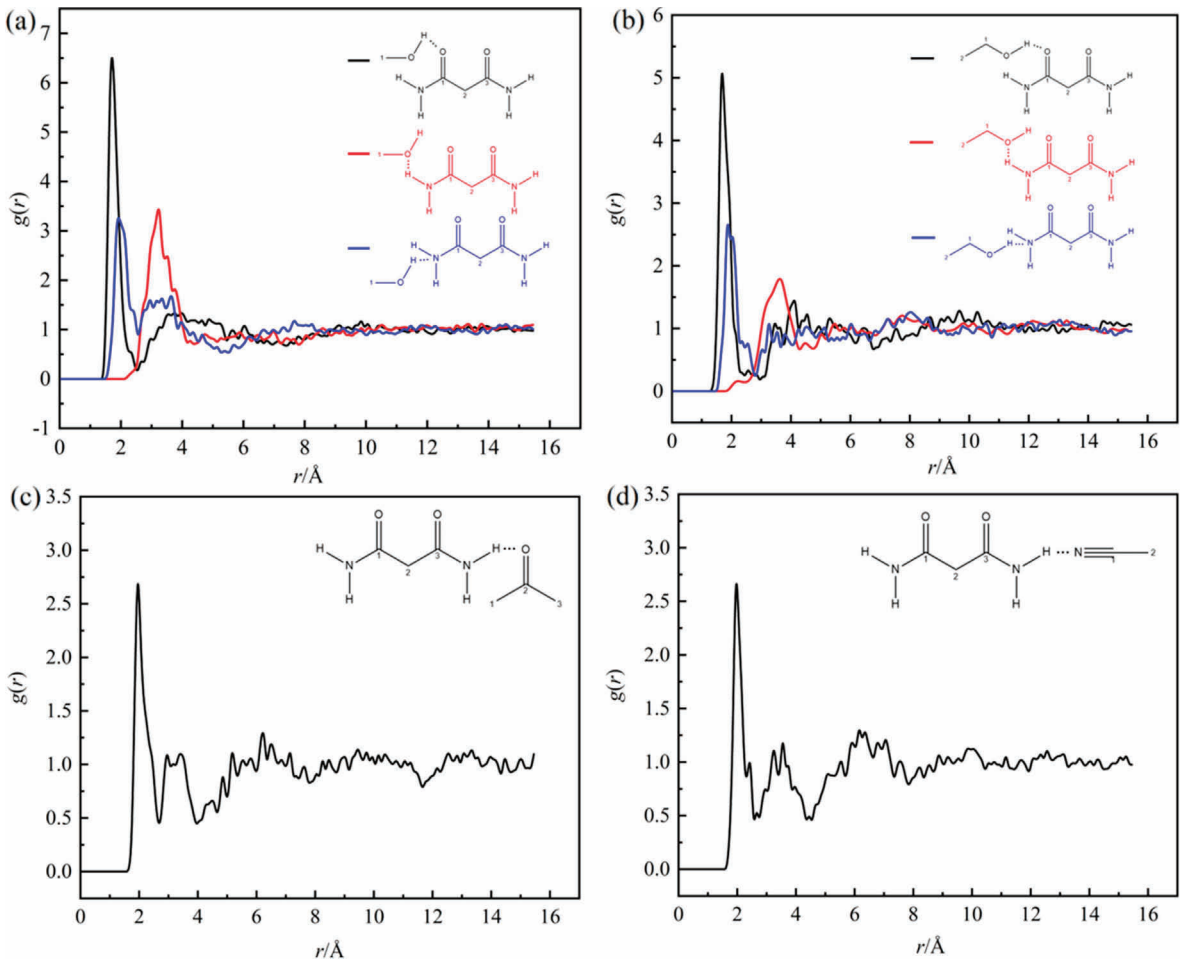

Fig. 10. The RDF analysis of the main hydrogen bonds between malonamide and (a) methanol, (b) ethanol, (c) acetone, (d) acetonitrile (1Å=0.1nm).

Table 1
The solvation free energy for different solvent systems.

Solvent	Water	Methanol	Ethanol	1-propanol	Acetone	Acetonitrile
Solvation free energy/kJ·mol^{-1}	−63.672	−62.453	−59.733	−58.459	−51.770	−50.423

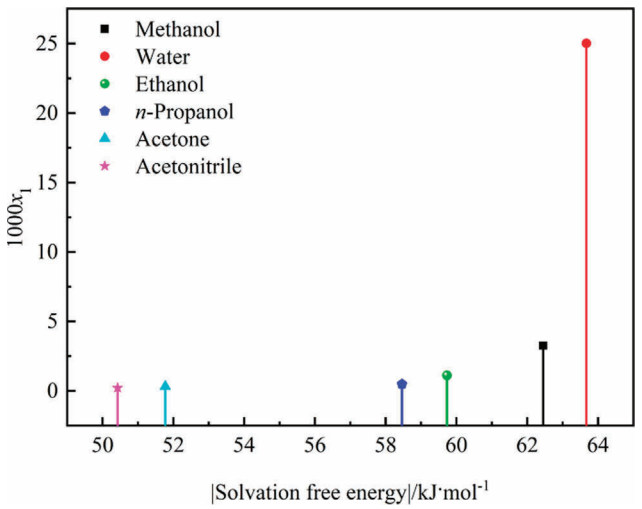

Fig. 11. The solubility of malonamide at 298.15 K as a function of the absolute values of solvation free energy.

ture, illustrated the increase in temperature favors the dissolution behavior.

Besides, the solvent effects on the equilibrium solubility were also investigated. The results indicate that "like dissolves like", "mass transfer" and "solvent–solute interactions" rules play a synergistic effect on the dissolution process. Furthermore, two molecular dynamic simulation: radial distribution function analysis and solvent free energy, were used to further explain the solubility rules. At last, the nucleation kinetics in methanol under four supercooling degree was measured at 293.15 K, in which the nucleation rate and effective interfacial energy were also calculated successfully.

Data Availability

Data will be made available on request.

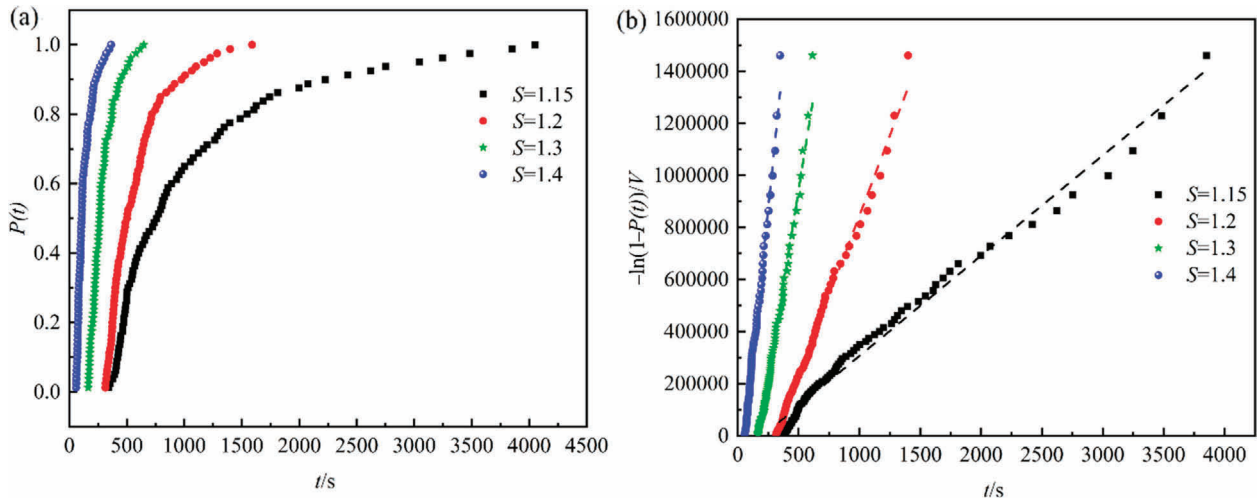

Fig. 12. (a) Induction time probability distributions of malonamide, (b) Induction time plotted as $-\ln(1-P(t))/V$ for malonamide at different supersaturations in methanol.

Table 2
The nucleation rate J and R^2 under different supersaturations.

Supersaturation	J/m^3 s^{-1}	R^2
1.15	385.0	0.986
1.2	1230.2	0.994
1.3	2924.2	0.988
1.4	4550.4	0.993

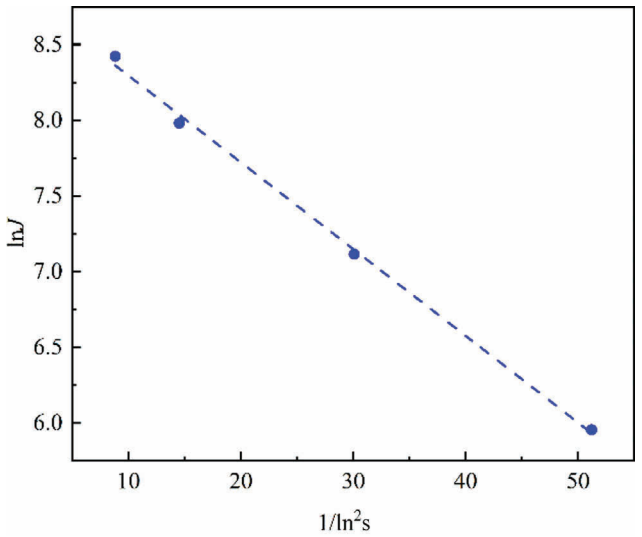

Fig. 13. The plot of ln$J$ with $1/\ln^2 S$.

Declaration of Competing Interest

The authors declare that they have no known competing financial interests or personal relationships that could have appeared to influence the work reported in this paper.

Acknowledgements

This work was financially supported by the Innovative Group Project of China (21621004) and Demonstration Project of Integration of Science, Education and Industry in Qilu University of Technology (2020KJC-ZD09).

Supplementary Material

Supplementary data to this article can be found online at https://doi.org/10.1016/j.cjche.2022.03.012.

Nomenclature

A, B, C	parameters of Apelblat equation
ARD	average relative deviation
a, b	fitting parameters of Van't Hoff equation
$\Delta_{mix}G$	mixing Gibbs energy, J·mol^{-1}
$\Delta_{fus}H$	melting enthalpy, kJ·mol^{-1}
$\Delta_{mix}H$	mixing enthalpy, J·mol^{-1}
J	nucleation rate, m^3 s^{-1}
k	Boltzmann constant, J·K^{-1}
M	molecular weight, g·mol^{-1}
m	mass, g
R	gas constant, J·mol^{-1}·K^{-1}
RMSD	root mean square deviation
S	supersaturation
$\Delta_{mix}S$	mixing entropy, J·mol^{-1}·K^{-1}
T	absolute temperature, K
T_m	melting point of malonamide, K
t	time, s
V	volume of the solution, ml
v	molecular volume of solute molecule, m^3
x	molar solubility
x^{cal}	calculated solubility
x^{exp}	experimental solubility

References

[1] M. Vatin, M. Duvail, P. Guilbaud, J.F. Dufrêche, Thermodynamics of malonamide aggregation deduced from molecular dynamics simulations, *J. Phys. Chem. B* 125 (13) (2021) 3409–3418.
[2] Y. Corvis, N. Guiblin, P. Espeau, Phase behavior and relative stability of malonamide polymorphs, *J. Phys. Chem. B* 118 (7) (2014) 1925–1931.
[3] E.Y. Cheung, M.L. Peterson, Reconciling thermal and structural data from the polymorphic transitions of malonamide, *Thermochim. Acta* 482 (1–2) (2009) 57–61.
[4] W. Hong, S.Z. Jia, Z.Q. Li, W.L. Li, Z.G. Gao, Solubility determination and thermodynamic correlation of chlorphenesin in 12 pure solvents from 288.15 to 328.15 K, *J. Chem. Eng. Data* 66 (1) (2021) 822–831.
[5] S.N. Zhang, N.N. Tian, S.Z. Jia, J. Yang, Y. Zhou, S.C. Du, Z.G. Gao, Solubility measurement and data correlation of pentaerythritol in four binary solvent systems at temperatures from 283.15 to 323.15 K, *J. Chem. Eng. Data* 66 (5) (2021) 2209–2217.

[6] Y.M. Shen, W.J. Liu, P.F. Shi, C. Wang, Solubility measurement and thermodynamic properties of sulfamonomethoxine in pure solvents and sulfamonomethoxine hydrate in acetone + water binary solvent at different temperature, *Chin. J. Chem. Eng.* 38 (2021) 196–204.
[7] Z.Q. Li, S.Z. Jia, Y. Gao, M.W. Wang, W. Hong, Z.G. Gao, J.B. Gong, Solid-liquid equilibrium behavior and thermodynamic analysis of *p*-aminobenzoic acid using experimental measurement and molecular dynamic simulation, *J. Mol. Liq.* 323 (2021) 114964.
[8] S.Z. Jia, K.K. Zhang, X.X. Wan, Z.G. Gao, J.B. Gong, S. Rohani, Effects of temperature and solvent properties on the liquid–solid phase equilibrium of γ-pyrazinamide, *J. Chem. Eng. Data* 65 (7) (2020) 3667–3678.
[9] Z.B. Mao, X.B. Sun, X.H. Luan, Y. Wang, G.J. Liu, Measurement and correlation of solubilities of adipic acid in different solvents, *Chin. J. Chem. Eng.* 17 (3) (2009) 473–477.
[10] L. Fang, Z.G. Gao, S.G. Wu, S.Z. Jia, J.K. Wang, S. Rohani, J.B. Gong, Ultrasound-assisted solution crystallization of fotagliptin benzoate: Process intensification and crystal product optimization, *Ultrason. Sonochem.* 76 (2021) 105634.
[11] Y.F. Cao, Q.W. Yang, H.B. Xing, Z.B. Bao, B.G. Su, Y.W. Yang, Q.L. Ren, Determination and correlation of solubility of nonivamide in different solvents, *Chin. J. Chem. Eng.* 22 (10) (2014) 1141–1144.
[12] H. Yan, Y.B. Liu, H.Y. Peng, J.H. Li, M.Y. Chen, J.B. Gong, Revealing dissolution behavior of *o*-methoxybenzoic acid in twelve pure solvents using thermodynamic analysis and molecular simulation, *J. Mol. Liq.* 336 (2021) 116242.
[13] C.Y. Zhao, J.W. Lin, Y. Gao, S.Z. Guo, R.L. Liu, S.G. Wu, Solid-liquid equilibrium behavior, thermodynamic analysis and molecular simulation of dimetridazole in twelve organic solvents, *J. Mol. Liq.* 336 (2021) 116252.
[14] W.W. Tang, H. Dai, Y. Feng, S.G. Wu, Y. Bao, J.K. Wang, J.B. Gong, Solubility of tridecanedioic acid in pure solvent systems: An experimental and computational study, *J. Chem. Thermodyn.* 90 (2015) 28–38.
[15] Z.X. Guo, J.W. Lin, P. Shi, Y.M. Ma, Y. Bao, Uncovering the solid-liquid equilibrium behavior of 6-Chloronicotinic acid in eleven pure solvents by thermodynamic analysis and molecular dynamic simulation, *J. Mol. Liq.* 331 (2021) 115757.
[16] M.W. Wang, Y. Liu, S.C. Du, Y.X. Zhao, S.Y. Liu, L.N. Zhou, S.G. Wu, Determining the solubility and understanding the solid-liquid equilibrium behavior of cyhalothric acid in eleven pure solvents, *J. Mol. Liq.* 300 (2020) 112365.
[17] R.R. Sun, Y.T. Wen, H.X. He, L. Yuan, Y.M. Wan, J. Sha, J.Y. Dong, Y. Li, T. Li, B.Z. Ren, Uridine in twelve pure solvents: Equilibrium solubility, thermodynamic analysis and molecular simulation, *J. Mol. Liq.* 330 (2021) 115663.
[18] Y. Liu, S.J. Xu, X. Zhang, W.W. Tang, J.B. Gong, Unveiling the critical roles of aromatic interactions in the crystal nucleation pathway of flufenamic acid, *Cryst. Growth Des.* 19 (12) (2019) 7175–7184.
[19] S.J. Xu, Y.F. Chen, J.B. Gong, J.K. Wang, Interplay between kinetics and thermodynamics on the probability nucleation rate of a urea–water crystallization system, *Cryst. Growth Des.* 18 (4) (2018) 2305–2315.
[20] G.L. Wang, Y.M. Liu, M.D. Liu, Y. Liu, J.B. Gong, H.C. Li, H.Q. Yin, S.G. Wu, The competition between solvent-solvent and solute-solvent act on the nucleation process of 4-(methylsulfonyl)benzaldehyde, *J. Mol. Liq.* 337 (2021) 116391.
[21] P.B. Lian, L.Z. Chen, D.Z. Huang, J.X. Xu, Z.S. Xu, C. Cao, J.X. Zhao, J.L. Wang, Crystallization thermodynamics of 2, 4(5)-dinitroimidazole in eleven pure solvents, *Chin. J. Chem. Eng.* 48 (2022) 236–243.
[22] F.L. Nordström, A.C. Rasmuson, Prediction of solubility curves and melting properties of organic and pharmaceutical compounds, *Eur. J. Pharm. Sci.* 36 (2–3) (2009) 330–344.
[23] F.F. Shen, L.Z. Chen, P.B. Lian, J.L. Wang, D.L. Cao, Solubility and metastable zone width measurement of 2,4-diaminobenzenesulfonic acid in (H_2SO_4 + H_2O) system, *Chin. J. Chem. Eng.* 44 (2022) 384–391.
[24] H. Renon, J.M. Prausnitz, Estimation of parameters for the NRTL equation for excess Gibbs energies of strongly nonideal liquid mixtures, *Ind. Eng. Chem. Proc. Des. Dev.* 8 (3) (1969) 413–419.
[25] H.Y. Yao, D.X. Yan, X.M. Lu, Q. Zhou, Y.N. Bao, J.L. Xu, Solubility determination and thermodynamic modeling of *bis*-2-hydroxyethyl terephthalate (BHET) in different solvents, *Chin. J. Chem. Eng.* 42 (2022) 91–103.
[26] X. Wu, S.S. Yang, S.M. Xu, X.J. Zhang, Y.J. Ren, Measurement and correlation of the solubility of sodium acetate in eight pure and binary solvents, *Chin. J. Chem. Eng.* 44 (2022) 474–484.
[27] W.L. Li, P. Shi, S. Wang, P. Yang, Y.X. Zhao, W.W. Tang, Solid-liquid phase equilibrium and thermodynamic analysis of metal dithiolene complex: The case of zinc dibutyldithiocarbamate, *J. Mol. Liq.* 284 (2019) 547–556.
[28] V. López-Mejías, J.W. Kampf, A.J. Matzger, Polymer-induced heteronucleation of tolfenamic acid: Structural investigation of a pentamorph, *J. Am. Chem. Soc.* 131 (13) (2009) 4554–4555.
[29] J.J. McKinnon, D. Jayatilaka, M.A. Spackman, Towards quantitative analysis of intermolecular interactions with Hirshfeld surfaces, *Chem. Commun. (Camb)* 37 (2007) 3814–3816.
[30] J.J. McKinnon, F.P.A. Fabbiani, M.A. Spackman, Comparison of polymorphic molecular crystal structures through hirshfeld surface analysis, *Cryst. Growth Des.* 7 (4) (2007) 755–769.
[31] J.R. Elliott, C.T. Lira, Introductory Chemical Engineering Thermodynamics, 2nd edition, Prentice Hall, Upper Saddle River, NJ, 2012.
[32] R.V. Orye, J.M. Prausnitz, Multicomponent equilibria-the Wilson equation, *Ind. Eng. Chem.* 57 (5) (1965) 18–26.
[33] W.J. Liu, Z.H. Bao, Y.M. Shen, T.T. Yao, H.J. Bai, X.Y. Jin, Solubility measurement and thermodynamic modeling of carbamazepine (form III) in five pure solvents at various temperatures, *Chin. J. Chem. Eng.* 33 (2021) 231–235.
[34] C.H. Gu, H. Li, R.B. Gandhi, K. Raghavan, Grouping solvents by statistical analysis of solvent property parameters: Implication to polymorph screening, *Int. J. Pharm.* 283 (1–2) (2004) 117–125.
[35] M.H. Abraham, Hydrogen bonding. 31. Construction of a scale of solute effective or summation hydrogen-bond basicity, *J. Phys. Org. Chem.* 6 (12) (1993) 660–684.
[36] I. Montes, C.Q. Lai, D. Sanabria, Like dissolves like: A guided inquiry experiment for organic chemistry, *J. Chem. Educ.* 80 (4) (2003) 447.
[37] J. Ouyang, J. Chen, I. Rosbottom, W.Q. Chen, M.X. Guo, J.Y.Y. Heng, Supersaturation and solvent dependent nucleation of carbamazepine polymorphs during rapid cooling crystallization, *CrystEngComm* 23 (4) (2021) 813–823.
[38] J.B. Ouyang, J. Chen, H.Q. Huang, L.M. Zhou, X. Huang, Solid-liquid equilibrium and dissolution thermodynamics of 4-methylumbelliferon in different solvents, *J. Mol. Liq.* 306 (2020) 112797.
[39] S.F. Jiang, J.H. ter Horst, Crystal nucleation rates from probability distributions of induction times, *Cryst. Growth Des.* 11 (1) (2011) 256–261.
[40] C. Brandel, J.H. ter Horst, Measuring induction times and crystal nucleation rates, *Faraday Discuss.* 179 (2015) 199–214.
[41] S.S. Kadam, S.A. Kulkarni, R. Coloma Ribera, A.I. Stankiewicz, J.H. ter Horst, H.J. M. Kramer, A new view on the metastable zone width during cooling crystallization, *Chem. Eng. Sci.* 72 (2012) 10–19.
[42] R.J. Davey, S.L.M. Schroeder, J.H. Ter Horst, Nucleation of organic crystals-A molecular perspective, *Angew. Chem. Int. Ed.* 52 (8) (2013) 2166–2179.
[43] D. Kashchiev, G.M. van Rosmalen, Review: Nucleation in solutions revisited, *Cryst. Res. Technol.* 38 (7–8) (2003) 555–574.